Journal Pre-proof

Immobilization of Ni–Pt nanoparticles on MIL-101/rGO composite for hydrogen evolution from hydrous hydrazine and hydrazine borane

Hongtao Zou, Shiliang Zhang, Xiaoling Hong, Qilu Yao, Yan Luo, Zhang-Hui Lu

PII: S0925-8388(20)31789-8

DOI: https://doi.org/10.1016/j.jallcom.2020.155426

Reference: JALCOM 155426

To appear in: *Journal of Alloys and Compounds*

Received Date: 15 January 2020

Revised Date: 23 April 2020

Accepted Date: 28 April 2020

Please cite this article as: H. Zou, S. Zhang, X. Hong, Q. Yao, Y. Luo, Z.-H. Lu, Immobilization of Ni–Pt nanoparticles on MIL-101/rGO composite for hydrogen evolution from hydrous hydrazine and hydrazine borane, *Journal of Alloys and Compounds* (2020), doi: https://doi.org/10.1016/j.jallcom.2020.155426.

Author contributions

Hongtao Zou: Methodology, Validation, Formal analysis, Investigation, Data curation, Writing-Review and Editing. **Shiliang Zhang:** Methodology, Investigation, Formal analysis, Writing-Original draft. **Xiaoling Hong:** Methodology, Validation, Formal analysis. **Qilu Yao:** Resources, Formal analysis, Review and Editing. **Yan Luo:** Formal analysis, Review and Editing. **Zhang-Hui Lu:** Conceptualization, Formal analysis, Resources, Supervision, Writing-Review and Editing, Project administration, Funding acquisition.

Graphical Abstract

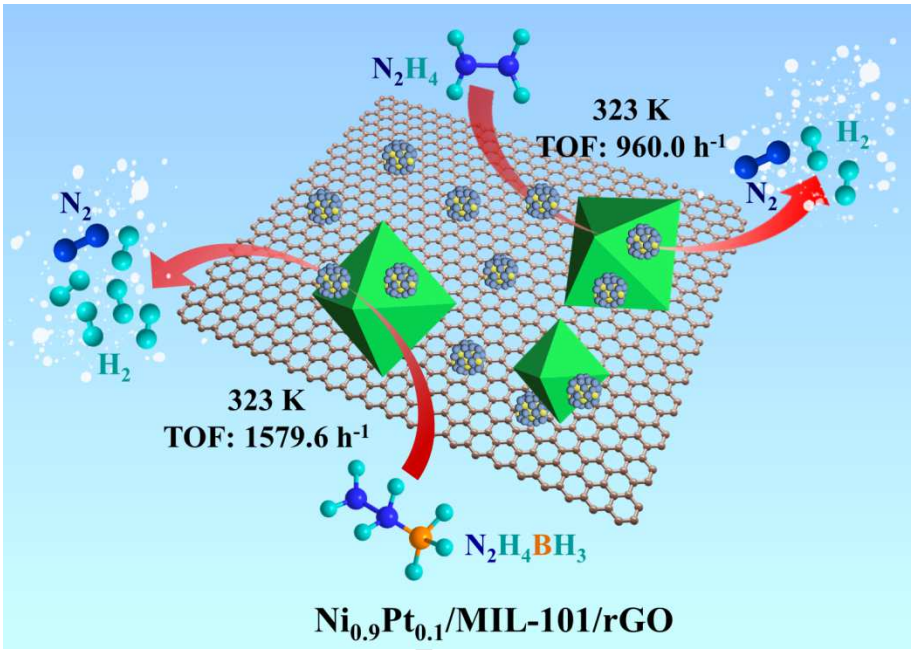

A low Pt-containing Ni-Pt nanocatalyst immobilized on MOF/rGO composite has been synthesized for hydrogen production from hydrous hydrazine and hydrazine borane.

Immobilization of Ni-Pt nanoparticles on MIL-101/rGO composite for hydrogen evolution from hydrous hydrazine and hydrazine borane

Hongtao Zou[a], Shiliang Zhang[a], Xiaoling Hong[a], Qilu Yao[a], Yan Luo[b], Zhang-Hui Lu[a,*]

[a]*Institute of Advanced Materials (IAM), College of Chemistry and Chemical Engineering, Jiangxi Normal University, Nanchang 330022, P.R. China*

[b]*College of Civil Aviation Safety Engineering, Civil Aviation Flight University of China, Guanghan 618307, P.R. China*

*Corresponding authors. E-mail: luzh@jxnu.edu.cn (Z.-H. Lu)

Abstract

As an ideal hydrogen supplier in liquid phase, hydrous hydrazine has gained a lot of attention for safe and efficient storage as well as transportation of hydrogen. Herein, a low Pt-containing Ni-Pt bimetallic catalyst immobilized on novel MIL-101/rGO composite has been prepared by a facile impregnation-reduction approach. Unexpectedly, the resultant $Ni_{0.9}Pt_{0.1}$/MIL-101/rGO catalyst exhibits optimal catalytic performance and 100% H_2 selectivity for hydrogen evolution from hydrous hydrazine under alkaline conditions at 323 K with, giving a turnover frequency (TOF) value of 960.0 h^{-1}, which is a relatively higher value ever reported heterogeneous catalysts. Even at room temperature, $Ni_{0.9}Pt_{0.1}$/MIL-101/rGO catalyst shows excellent catalytic activity for dehydrogenation of hydrazine as well as hydrazine borane. In addition, the $Ni_{0.9}Pt_{0.1}$/MIL-101/rGO catalyst also exhibits excellent durability. Even after eight recycles, the catalytic activity is no significant decrease, and the H_2 selectivity still remains 100%.

Keywords: Hydrazine; Nanoparticle; Metal-organic framework; Graphene; Hydrogen evolution

1. Introduction

Hydrogen energy, as a highly-efficient, sustainable, pollution-free, and abundant source of secondary energy, has attracted increasing interest [1-3]. However, safely storing and transporting hydrogen remains a grand challenge for the achievement of hydrogen economy society [4-6]. Recently, more and more efforts have been made to study chemical hydrides as efficient carriers for chemical hydrogen storage [7-9]. Hydrous hydrazine ($N_2H_4 \cdot H_2O$) has great potential as a promising liquid chemical hydrogen storage material for storage and transportation of hydrogen, because of its high hydrogen content (8.0 wt%), stable liquid state, nontoxicity, and clean emissions (only nitrogen as byproduct via equation (1)) [10-12]. To this end, the incomplete decomposition of hydrazine to ammonia (NH_3) via equation (2) should be avoided [13-15]. Consequently, the key is to develop simple and effective strategies to synthesize a high-efficient and low-cost heterogeneous catalyst for complete dehydrogenation of hydrazine.

$$N_2H_4(l) \rightarrow N_2(g) + 2H_2(g) \quad (1)$$

$$3N_2H_4(l) \rightarrow N_2(g) + 4NH_3(g) \quad (2)$$

In recent years, noble-metal-containing nickel-based bimetallic heterogeneous nanocatalysts, such as Ni-Rh [16-18], Ni-Pt [19-21], Ni-Ir [22, 23], and Ni-Pd [24-26], have been synthesized and explored for dehydrogenation of hydrazine. Numerous studies have demonstrated that Ni-Pt catalysts possess excellent catalytic properties for

hydrazine decomposition [27-29]. Generally, organic surfactants could help to control and stabilize the metal nanoparticles (NPs), but the metal active sites may be blocked after involved organic stabilizers, leading to a deterioration of catalytic performance [30, 31]. Loading the metal NPs onto the inorganic support with large specific surface area could stabilize the metal NPs without aggregation [29, 32]. Recently, metal-organic frameworks (MOFs) and graphene oxide (GO) have been considered as promising carriers due to their unique structure and properties [33-39]. To be noted, lots of studies find that the catalytic performance and stability of MOFs/GO composites, to some extent, have been enhanced in comparison with pure MOFs and GO [40-43].

Herein, low noble-metal-containing Ni-Pt NPs have been immobilized on MIL-101/rGO composite using the facile impregnation-reduction method without the help of surfactant. Interestingly, the resultant $Ni_{0.9}Pt_{0.1}$/MIL-101/rGO shows excellent catalytic performances and 100% H_2 selectivity for decomposition of hydrazine and hydrazine borane at 323 K, affording turnover frequency (TOF) values of 960.0 and 1579.9 h^{-1}, respectively.

2. Materials and methods

2.1. Materials

Graphite powder (J&K Chemical, 99%), sulfuric acid (H_2SO_4, Nanchang Xinguang Fine Chemical Works, 98%), phosphorus pentoxide (P_2O_5, Tianjin Fuchen Chemical Reagent, 98%), potassium permanganate ($KMnO_4$, Nanchang Xinguang Fine Chemical Works, >99.5%), potassium persulfate ($K_2S_2O_8$, Tianjin Fuchen Chemical Reagent,

99.5%), *n*-pentane (C_5H_{12}, Sigma-Aldrich, 99.5%), hydrogen peroxide (H_2O_2, Tianjin Fuchen Chemical Reagent, 30%), chromium nitrate nonahydrate ($Cr(NO_3)_3·9H_2O$, Aladdin, 99%), aqueous hydrofluoric acid (HF, Aladdin, 40 wt%), terephthalic acid (H_2BDC, Aladdin, 99%), nickel (II) chloride hexahydrate ($NiCl_2·6H_2O$, Aladdin, 98%), potassium (II) tetrachloroplatinate (K_2PtCl_4, J&K Chemical, 99.95%), hydrous hydrazine ($N_2H_4·H_2O$, Sigma-Aldrich, 98%), 1,4-dioxane ($C_4H_8O_2$, J&K Chemical, 99.8%), sodium borohydride ($NaBH_4$, Acros, 98%), sodium hydroxide (NaOH, Tianjin Fuchen Chemical Reagent, 96%), and hydrazine hemisulfate salt ($N_2H_4·1/2H_2SO_4$, Sigma-Aldrich, 99.5%) were from commercial sources and used as received. Hydrazine borane ($N_2H_4BH_3$) was prepared according to the procedure reported in literature [25, 44].

2.2. Synthesis of MIL-101/GO composite

MIL-101/GO composite was synthesized using a similar method according to the procedure for synthesis of MIL-101 [27, 45]. 4.0 g of $Cr(NO_3)_3·9H_2O$, 400 mg of as-prepared GO, 0.5 mL of HF, and 1.6 g of H_2BDC were dispersed in 70 mL water. Then, the above suspension was heated to 493 K and maintained for 8 h. After the resultant suspension was cooled to room temperature, the product was washed with water and ethanol. To further remove the un-reacted H_2BDC, the as-synthesized sample was soaked in ethanol solution at 353 K for 24 h, then in NH_4F (1.0 M) solution at 343 K for another 24 h. Finally, the resulting sample was washed with ethanol three times and followed by drying under vacuum at 323 K overnight.

2.3. Synthesis of NiPt/MIL-101/rGO

NiPt/MIL-101/rGO catalyst was synthesized by a facile impregnation-reduction approach. Typically, 65 mg of as-synthesized MIL-101/GO composite, 0.09 mmol of $NiCl_2 \cdot 6H_2O$, and 0.01 mmol of K_2PtCl_4 were ultrasonically dispersed in 5 mL water. The resultant suspension was keep stirring for 6 h to impregnate the metal salts. Subsequently, 30 mg of $NaBH_4$ was added into the above mixture to obtain $Ni_{0.9}Pt_{0.1}$/MIL-101/rGO nanocatalyst. Ni_xPt_{1-x}/MIL-101/rGO nanocatalysts with other different molar ratios of Ni/Pt (0:1, 0.3:0.7, 0.5:0.5, 0.7:0.3, and 1:0) were prepared following the same procedure except that $NiCl_2 \cdot 6H_2O$ and K_2PtCl_4 with different molar ratios were added. $Ni_{0.9}Pt_{0.1}$/MIL-101/rGO nanocatalysts with different metal loadings were also prepared by changing the addition contents of MIL-101/GO supports. Additionally, the $Ni_{0.9}Pt_{0.1}$/rGO and $Ni_{0.9}Pt_{0.1}$/MIL-101 nanocatalysts were prepared using the similar method above, by replaced the support material to GO and MIL-101, respectively.

2.4. Catalytic activities

The catalytic reaction equipment used to measure the H_2/N_2 evolution from hydrous hydrazine or hydrazine borane is similar to that previously reported [46]. Typically, 5 mL aqueous suspension containing the obtained catalyst and 5.0 mmol NaOH was added into the reactor. One port of the reactor was used for measure the volume of the produced gas, while the other port was directly used to introduce hydrous hydrazine (2.0 mmol) or hydrazine borane (1.0 mmol). A trap filled with hydrochloric acid (1.0 M) was placed between the reactor and gas buret to absorb any released NH_3. The H_2 selectivity (α) toward hydrogen production from hydrous hydrazine could be calculated on the basis of equation (3), which can be deduced from equations (1) and (2). The H_2 selectivity (β)

toward hydrogen generation from hydrazine borane could be evaluated according to equation (4), which can be deduced from equations (1), (2), and equation (5).

$$N_2H_4 \rightarrow 2\alpha H_2 + (2\alpha+1)/3N_2 + 4(1-\alpha)/3NH_3 \quad (3)$$

$$N_2H_4BH_3 + 3H_2O \rightarrow B(OH)_3 + (3+2\beta)H_2 + (2\beta+1)/3N_2 + 4(1-\beta)/3NH_3 \quad (4)$$

$$N_2H_4BH_3(s) + 3H_2O(l) \rightarrow N_2H_4(l) + B(OH)_3(l) + 3H_2(g) \quad (5)$$

As NH_3 is highly solution in hydrochloric acid and water, the gas volume measured by the gas buret contains only hydrogen and nitrogen, from which the molar ratio $\lambda = n(H_2+N_2)/n(N_2H_4)$ and $\gamma = n(H_2+N_2)/n(N_2H_4BH_3)$ could be calculated [17-20]. Therefore, the H_2 selectivity α and β could be calculated through equations (6) and (7), respectively.

$$\alpha = \frac{3\lambda - 1}{8}\left[\lambda = \frac{n(H_2 + N_2)}{n(N_2H_4)}\left(\frac{1}{3} \le \lambda \le 3\right)\right] \quad (6)$$

$$\beta = \frac{3\gamma - 10}{8}\left[\gamma = \frac{n(H_2 + N_2)}{n(N_2H_4BH_3)}\left(\frac{10}{3} \le \gamma \le 6\right)\right] \quad (7)$$

3. Results and discussion

3.1. Synthesis and characterization of catalysts

The procedure of immobilized Ni-Pt NPs on MIL-101/rGO composite is illustrated in Scheme 1. Briefly, the as-prepared GO was hydrothermally treated together with H_2BDC and $Cr(NO_3)_3{\cdot}9H_2O$ to get MIL-101/GO composite material. The resultant MIL-101/GO composite was dispersed in water through ultrasound, followed by addition of $NiCl_2$ and K_2PtCl_4. Finally, $NaBH_4$ as the reducing agent was added to obtain the NiPt/MIL-101/rGO nanocatalysts. Among all the as-prepared catalysts, $Ni_{0.9}Pt_{0.1}$/MIL-101/rGO with 10.0 wt% Ni-Pt loading was selected as a model catalyst for

full characterization, because of its excellent dehydrogenation catalytic performance.

The crystal structures of GO, MIL-101, MIL-101/GO, Ni/MIL-101/rGO, NiPt/MIL-101/rGO, and Pt/MIL-101/rGO samples were characterized by power XRD (Fig. 1 and Fig. S1). As shown in Fig. 1a and Fig. S1, the characteristic diffraction peaks of MIL-101 can be apparently observed in MIL-101/GO composite, indicating the successful formation of MIL-101 crystals on GO [29, 47]. This observation has been further confirmed by FTIR and Raman spectra (Fig. S2). The characteristic diffraction peaks of MIL-101 crystal are still retained after loading of metal NPs (Fig. 1a), suggesting the crystalline structure of MIL-101 is stable during catalyst preparation. Additionally, the wide-angle XRD pattern of NiPt/MIL-101/rGO shows a broad and weak diffraction peaks at 2θ = 42.7° (Fig. 1b), which is located between the Ni (111) (JCPDS no. 04-0850) and Pt (111) (JCPDS no. 04-0802), clearly demonstrating the formation of the Ni-Pt alloy [21]. Furthermore, XPS measurements were performed to reveal the elemental compositions and electronic structure of $Ni_{0.9}Pt_{0.1}$/MIL-101/rGO nanocatalyst. The survey XPS full spectrum for $Ni_{0.9}Pt_{0.1}$/MIL-101/rGO shows the co-existence of Ni, Pt, Cr, C, and O (Fig. S3). As shown in Fig. 2a, the binding energies for Ni $2p_{3/2}$ and Ni $2p_{1/2}$ at 852.9 and 870.1 eV are clearly observed in Ni 2p XPS spectrum, which could be assigned to states of Ni^0 [48]. For Pt 4f XPS spectrum, the binding energies for Pt $4f_{7/2}$ and Pt $4f_{5/2}$ at 71.6 and 74.9 eV are attributed to states of Pt^0 (Fig. 2b) [32]. In addition, the binding energies for Ni $2p_{3/2}$ and Ni $2p_{1/2}$ at 853.5 and 873.5 eV are corresponded to Ni^{2+}, which could be explained by the surface oxidation of Ni during the sample preparation process for XPS test [49]. Besides, the Ni $2p_{3/2}$ peaks at

about 858.2 eV and Ni $2p_{1/2}$ peak at about 877.0 eV are assigned to the satellite peaks of Ni [15]. These results suggest that Ni-Pt NPs composed of metallic Ni, metallic Pt and a little amount of oxidized Ni have been successfully formed on MIL-101/rGO composite.

The SEM images present that original GO is a thin and wrinkled lamellar structure (Fig. 3a), while MIL-101 material appears a regular octahedral morphology (Fig. 3b). The detail morphology of $Ni_{0.9}Pt_{0.1}$/MIL-101/rGO nanocatalyst was investigated via TEM. As shown in Fig. 3c,d, and Fig. S4, the Ni-Pt NPs (~9.2 nm, Fig. S5) are well dispersed on MIL-101/rGO composite surface. The high resolution TEM image shows the lattice fringes of $Ni_{0.9}Pt_{0.1}$/MIL-101/rGO nanocatalyst with d-spacing of 0.218 nm (Fig. 3e), confirming the formation of Ni-Pt (111) planes [27, 50]. Moreover, the SAED pattern displays a diffraction ring radius with 4.58 1/nm (Fig. 3f), further implying that the successful formation the structure of Ni-Pt alloy [13]. The corresponding EDX analysis of $Ni_{0.9}Pt_{0.1}$/MIL-101/rGO further indicates the existence of Ni, Pt, Cr, C, and O elements (Fig. S6).

The Brunauer-Emmett-Teller (BET) specific surface areas of as-prepared samples were determined via nitrogen adsorption-desorption isotherms measurements after dehydration under vacuum at 373 K for 8 h. As shown in Fig. 4, the BET specific surface area for MIL-101/GO composite is measured to be 3200 $m^2 \cdot g^{-1}$, which is larger than that of pure MIL-101 (2891 $m^2 \cdot g^{-1}$). The pure GO sample prepared in the present work shows a very low specific surface area of only 18 $m^2 \cdot g^{-1}$ (Fig. S7), which is much lower than that of the real specific surface area of GO dispersed in the solution, probably due to the overlapping of graphene sheets within the self-aggregation during the drying process

[17]. To be noted, there is a distinctly adsorption hysteresis loop in MIL-101/GO composite, revealing that a new pore space is formed between MIL-101 crystal and GO in the composite [45]. In addition, the specific surface area of the as-prepared $Ni_{0.9}Pt_{0.1}$/MIL-101/rGO nanocatalyst (1371 $m^2 \cdot g^{-1}$) is lower than that of MIL-101/GO, revealing that a part of the pores and/or defects were occupied by Ni-Pt NPs [51]. This MIL-101/GO composite with high specific surface area is typically beneficial for mass transfer processes, which can largely increase the catalytic dehydrogenation reaction dynamics. On the other hand, the porous surface structure could offer steric restriction to confine and prevent the growth of the metal NPs [29, 33-35].

3.2. Catalytic performances

The catalytic performances for hydrazine decomposition were investigated under alkaline conditions. As presented in Fig. 5, the $Ni_{0.9}Pt_{0.1}$/MIL-101/rGO nanocatalyst performs the best dehydrogenation activity of hydrazine, releasing 3.0 equivalents of (N_2+H_2) in only 3.0 min with a TOF value of 960.0 h^{-1}, which is a relatively higher value over heterogeneous catalysts reported previously for this reaction (Table S1) [8, 11, 14, 17, 22, 23, 29, 52-55]. For comparison, the activities of $Ni_{0.9}Pt_{0.1}$/MIL-101, $Ni_{0.9}Pt_{0.1}$/rGO, pure $Ni_{0.9}Pt_{0.1}$ NPs, and MIL-101/GO were also measured. Clearly, all these reference catalysts exhibit much lower catalytic activities than that of $Ni_{0.9}Pt_{0.1}$/MIL-101/rGO, giving the corresponding TOF values of 452.8, 158.5, 97.3, and 0 h^{-1}, respectively. This remarkable catalytic activity could be directly attributed to its unique structure and high specific surface area.

Then, the effect of Ni/Pt molar ratios in NiPt/MIL-101/rGO nanocatalysts on the

catalytic performances for hydrazine decomposition was carefully investigated. As shown in Fig. 6, the activities and selectivity versus Ni/Pt molar ratios show typical volcano-shaped profile. The monometallic Ni/MIL-101/rGO exhibits a poor catalytic performance and H_2 selectivity, while the monometallic Pt/MIL-101/rGO is almost inactive. Interestingly, after addition of Ni to form Ni-Pt alloy, the bimetallic catalysts exhibit a much higher activity and selectivity compared with their monometallic counterparts. With the increasing of Ni/Pt molar ratios, the activities of hydrazine dehydrogenation are increased at first and the optimum catalysis can be obtained by using a Ni/Pt ratio of 0.9:0.1. A further increase of Ni/Pt molar ratios leads to the loss of catalytic activities. Meanwhile, ICP-AES analysis confirmed that the Ni/Pt ratios of as-prepared catalysts match the predesigned trend and the actual contents of Ni and Pt are close to the nominal values (Table S2). To reveal the optimal metal loadings, the catalytic activities $Ni_{0.9}Pt_{0.1}$/MIL-101/rGO nanocatalysts with the different loadings of Ni-Pt NPs (5.0, 7.5, 10.0, and 12.5 wt%) have been also investigated (Fig. S8). Results show that $Ni_{0.9}Pt_{0.1}$/MIL-101/rGO nanocatalyst with 10.0 wt% total Ni-Pt loading exhibits the highest catalytic activity for hydrazine decomposition. These enhanced catalytic performances might be not only attributed to the intermetallic synergic effects, but also the metal-support interaction [51, 56].

To investigate the effect of NaOH, the catalytic performances have been tested with different NaOH concentrations (Fig. S9). $Ni_{0.9}Pt_{0.1}$/MIL-101/rGO shows poor activity in the absence of NaOH with only 2.3 equivalents of (H_2 + N_2) generated in 29.2 min. As the NaOH concentration increased to 1.0 M, the catalytic activity is significantly improved.

When the NaOH concentration is further increased, it has a negative effect, revealing that the optimal NaOH concentration was 1.0 M. As demonstrated in Fig. S10, pure NaOH has no catalytic activity, indicating that NaOH is acted as a promoter, not a catalyst. The alkaline environment not only promote the rate-determining step of hydrazine decomposition into N_2 and H_2 ($N_2H_4 \rightarrow N_2H_3^* + H^*$), but also inhibit the generation of byproduct NH_3, which raises the H_2 selectivity [28, 51, 57].

Furthermore, the effect of reaction temperature on hydrazine dehydrogenation over optimized $Ni_{0.9}Pt_{0.1}$/MIL-101/rGO nanocatalyst was investigated. As shown in Fig. 7a, the catalytic activities are rapidly enhanced with increasing the reaction temperature. The corresponding TOF values are calculated to be 180.5, 274.6, 638.3, 960.0, and 1363.6 h^{-1} at 298, 308, 313, 323, and 333 K, respectively (Fig. 7b). According to the rate constant *k* of the hydrazine decomposition reaction at different temperatures, the Arrhenius plot of ln *k* versus 1/T was plotted in the inset of Fig. 7a, the activation energy (E_a) of $Ni_{0.9}Pt_{0.1}$/MIL-101/rGO nanocatalyst for hydrazine decomposition is 50.6 kJ·mol^{-1}. This value is much lower than most of the heterogeneous catalysts reported previously for this reaction (Table S2) [8, 11, 14, 17, 22, 23, 29, 52-55].

Recently, hydrazine borane ($N_2H_4BH_3$), as an emerging chemical hydrogen storage material, has triggered tremendous attention because of its very high hydrogen density (15.4 wt%) and satisfactory stability under ambient conditions. The complete hydrogen release from hydrazine borane can produce 5.0 equivalents of H_2 ($N_2H_4BH_3$ (s) + $3H_2O$ → $B(OH)_3$ (l) + N_2 (g) + $5H_2$ (g)) [58-61]. Considering its superior catalytic properties for hydrazine decomposition, this optimized $Ni_{0.9}Pt_{0.1}$/MIL-101/rGO nanocatalyst was also

used to hydrogen evolution from hydrazine borane at the same condition. As presented in Fig. 7c, the influence of reaction temperature on dehydrogenation reaction rate of hydrazine borane was also evaluated. Hydrogen generation from hydrazine borane decomposition can be finished within 14.7, 4.9, 4.1, 1.9, and 1.1 min at 298, 308, 313, 323, and 333 K, respectively, corresponding to TOF values of 203.0, 606.1, 717.7, 1578.9, and 2654 h^{-1} (Fig. 7d). These values are relatively high values among the reported heterogeneous catalysts [13, 17, 23, 25, 27, 44, 48, 58-60]. The activation energies for BH_3 group hydrolysis (E_{a1}, Part 1) and N_2H_4 moiety decomposition (E_{a2}, Part 2) of hydrazine borane are determined to be 17.6 and 56.4 $kJ \cdot mol^{-1}$ (Fig. 7c, inset), respectively. We further examine briefly the durability of $Ni_{0.9}Pt_{0.1}$/MIL-101/rGO nanocatalyst to the decomposition reaction of hydrazine and hydrazine borane. As presented in Fig. 8, the $Ni_{0.9}Pt_{0.1}$/MIL-101/rGO nanocatalyst shows excellent durability. Even after eight recycles, the catalytic activity is no significant decreased, and the H_2 selectivity still remains 100%.

4. Conclusions

In summary, we have reported a simple impregnation-reduction strategy for immobilization of low noble-metal-containing bimetallic Ni-Pt NPs on novel MIL-101/rGO composite. Unexpectedly, the resultant $Ni_{0.9}Pt_{0.1}$/MIL-101/rGO nanocatalyst exhibits excellent catalytic activity and 100% H_2 selectivity for hydrogen evolution from hydrous hydrazine at 323 K under alkaline conditions. The corresponding TOF reaches 960.0 h^{-1}, which is much higher than most of the

heterogeneous catalysts reported to date. The characterization results revealed that the Ni-Pt NPs were successfully immobilized on MIL-101/rGO composite with unique structure and high specific surface area. In addition, $Ni_{0.9}Pt_{0.1}$/MIL-101/rGO nanocatalyst is also beneficial to high-extent dehydrogenation of hydrazine borane under the same condition, achieving the 5.0 equivalents of H_2 within 1.9 min. What's more, even after eight recycles of the catalytic process, the H_2 selectivity is maintained and their initial catalytic activity shows no significant decrease. Such unique strategy via synthesizing some unique structure and high specific surface area composite to support metal NPs might benefit to design a series of novel nanocatalysts for the wide practical application prospect in various catalytic fields.

Acknowledgments

This work was financially supported by the National Natural Science Foundation of China (Nos. 21763012 and 21802056) and the Natural Science Foundation of Jiangxi Province of China (No. 20192BAB203009).

References

[1] L. Schlapbach, A. Zuttel, Hydrogen-storage materials for mobile applications, Nature, 414 (2001) 353-358. http://doi.org/10.1038/35104634.

[2] A. Sartbaeva, V.L. Kuznetsov, S.A. Wells, P.P. Edwards, Hydrogen nexus in a sustainable energy future, Energy Environ. Sci., 1 (2008) 79-85. http://doi.org/10.1039/b810104n.

[3] Q.L. Zhu, Q. Xu, Liquid organic and inorganic chemical hydrides for high-capacity

hydrogen storage, Energy Environ. Sci., 8 (2015) 478-512. http://doi.org/10.1039/c4ee03690e.

[4] Q.L. Yao, W.M. Shi, G. Feng, Z.H. Lu, X.L. Zhang, D.J. Tao, D.J. Kong, X.S. Chen, Ultrafine Ru nanoparticles embedded in SiO_2 nanospheres: Highly efficient catalysts for hydrolytic dehydrogenation of ammonia borane, J. Power Sources, 257 (2014) 293-299. http://doi.org/10.1016/j.jpowsour.2014.01.122.

[5] T. He, P. Pachfule, H. Wu, Q. Xu, P. Chen, Hydrogen carriers, Nat. Rev. Mater., 1 (2016) 16059. http://doi.org/10.1038/natrevmats.2016.59.

[6] D.S. Lu, J.H. Li, C.H. Lin, J.Y. Liao, Y.F. Feng, Z.T. Ding, Z.W. Li, Q.B. Liu, H. Li, A simple and scalable route to synthesize $Co_xCu_{1-x}Co_2O_4$@$Co_yCu_{1-y}Co_2O_4$ yolk-shell microspheres, a high-performance catalyst to hydrolyze ammonia borane for hydrogen production, Small, 15 (2019) 1805460. http://doi.org/10.1002/smll.201805460.

[7] Q.L. Yao, Z.H. Lu, W. Huang, X.S. Chen, J. Zhu, High Pt-like activity of the Ni-Mo/graphene catalyst for hydrogen evolution from hydrolysis of ammonia borane, J. Mater. Chem. A, 4 (2016) 8579-8583. http://doi.org/10.1039/c6ta02004f.

[8] S.N. Oliaee, C.L. Zhang, S.Y. Hwang, H.M. Cheung, Z.M. Peng, Hydrogen production via hydrazine decomposition on model platinum-nickel nanocatalyst with a single (111) facet, J. Phys. Chem. C, 120 (2016) 9764-9772. http://doi.org/10.1021/acs.jpcc.6b00815.

[9] A.L. Jin, Y.S. Jia, C.F. Chen, X. Liu, J.Z. Jiang, X.S. Chen, F. Zhang, Efficient photocatalytic hydrogen evolution on band structure tuned polytriazine/heptazine

based carbon nitride heterojunctions with ordered needle-like morphology achieved by an in situ molten salt method, J. Phys. Chem. C, 121 (2017) 21497-21509. http://doi.org/10.1021/acs.jpcc.7b07243.

[10] S.K. Singh, X.B. Zhang, Q. Xu, Room-temperature hydrogen generation from hydrous hydrazine for chemical hydrogen storage, J. Am. Chem. Soc., 131 (2009) 9894-9895. http://doi.org/10.1021/ja903869y.

[11] Y.J. Zhong, H.B. Dai, Y.Y. Jiang, D.M. Chen, M. Zhu, L.X. Sun, P. Wang, Highly efficient Ni@Ni-Pt/La2O_3 catalyst for hydrogen generation from hydrous hydrazine decomposition: Effect of Ni-Pt surface alloying, J. Power Sources, 300 (2015) 294-300. http://doi.org/10.1016/j.jpowsour.2015.09.071.

[12] L. He, B.L. Liang, Y.Q. Huang, T. Zhang, Design strategies of highly selective nickel catalysts for H_2 production via hydrous hydrazine decomposition: a review, Natl. Sci. Rev., 5 (2018) 356-364. http://doi.org/10.1093/nsr/nwx123.

[13] Z.J. Zhang, Z.H. Lu, X.S. Chen, Ultrafine Ni-Pt alloy nanoparticles grown on graphene as highly efficient catalyst for complete hydrogen generation from hydrazine borane, ACS Sustainable Chem. Eng., 3 (2015) 1255-1261. http://doi.org/10.1021/acssuschemeng.5b00250.

[14] W. Kang, A. Varma, Hydrogen generation from hydrous hydrazine over Ni/CeO_2 catalysts prepared by solution combustion synthesis, Appl. Catal. B: Environ., 220 (2018) 409-416. http://doi.org/10.1016/j.apcatb.2017.08.053.

[15] H.T. Zou, Q.L. Yao, M.L. Huang, M.H. Zhu, F. Zhang, Z.H. Lu, Noble-metal-free NiFe nanoparticles immobilized on nano $CeZrO_2$ solid solutions for highly efficient

hydrogen production from hydrous hydrazine, Sustainable Energy Fuels, 3 (2019) 3071-3077. http://doi.org/10.1039/c9se00547a.

[16] J. Wang, X.B. Zhang, Z.L. Wang, L.M. Wang, Y. Zhang, Rhodium-nickel nanoparticles grown on graphene as highly efficient catalyst for complete decomposition of hydrous hydrazine at room temperature for chemical hydrogen storage, Energy Environ. Sci., 5 (2012) 6885-6888. http://doi.org/10.1039/c2ee03344e.

[17] Z.J. Zhang, Z.H. Lu, H.L. Tan, X.S. Chen, Q.L. Yao, CeO_x-modified RhNi nanoparticles grown on rGO as highly efficient catalysts for complete hydrogen generation from hydrazine borane and hydrazine, J. Mater. Chem. A, 3 (2015) 23520-23529. http://doi.org/10.1039/c5ta06197k.

[18] J.M. Chen, Q.L. Yao, J. Zhu, X.S. Chen, Z.H. Lu, Rh-Ni nanoparticles immobilized on $Ce(OH)CO_3$ nanorods as highly efficient catalysts for hydrogen generation from alkaline solution of hydrazine, Int. J. Hydrogen Energy, 41 (2016) 3946-3954. http://doi.org/10.1016/j.ijhydene.2015.12.158.

[19] S.K. Singh, Q. Xu, Bimetallic Ni-Pt nanocatalysts for selective decomposition of hydrazine in aqueous solution to hydrogen at room temperature for chemical hydrogen storage, Inorg. Chem., 49 (2010) 6148-6152. http://doi.org/10.1021/ic1007654.

[20] Y.N. Men, J. Su, X.L. Wang, P. Cai, G.Z. Cheng, W. Luo, NiPt nanoparticles supported on CeO_2 nanospheres for efficient catalytic hydrogen generation from alkaline solution of hydrazine, Chin. Chem. Lett., 30 (2019) 634-637.

http://doi.org/10.1016/j.cclet.2018.11.010.

[21] A. Kumar, X.C. Yang, Q. Xu, Ultrafine bimetallic Pt-Ni nanoparticles immobilized on 3-dimensional N-doped graphene networks: a highly efficient catalyst for dehydrogenation of hydrous hydrazine, J. Mater. Chem. A, 7 (2019) 112-115. http://doi.org/10.1039/c8ta09003c.

[22] L. He, Y.Q. Huang, X.Y. Liu, L. Li, A.Q. Wang, X.D. Wang, C.Y. Mou, T. Zhang, Structural and catalytic properties of supported Ni-Ir alloy catalysts for H_2 generation via hydrous hydrazine decomposition, Appl. Catal. B: Environ. , 147 (2014) 779-788. http://doi.org/10.1016/j.apcatb.2013.10.022.

[23] X.L. Hong, Q.L. Yao, M.L. Huang, H.X. Du, Z.H. Lu, Bimetallic NiIr nanoparticles supported on lanthanum oxy-carbonate as highly efficient catalysts for hydrogen evolution from hydrazine borane and hydrazine, Inorg. Chem. Front. , 6 (2019) 2271-2278. http://doi.org/10.1039/c9qi00848a.

[24] S.K. Singh, Y. Iizuka, Q. Xu, Nickel-palladium nanoparticle catalyzed hydrogen generation from hydrous hydrazine for chemical hydrogen storage, Int. J. Hydrogen Energy, 36 (2011) 11794-11801. http://doi.org/10.1016/j.ijhydene.2011.06.069.

[25] Q.L. Yao, K.K. Yang, W.D. Nie, Y.X. Li, Z.H. Lu, Highly efficient hydrogen generation from hydrazine borane via a MoO_x-promoted NiPd nanocatalyst, Renewable Energy, 147 (2020) 2024-2031. http://doi.org/10.1016/j.renene.2019.09.144.

[26] K. Yang, K.K. Yang, S.L. Zhang, Y. Luo, Q.L. Yao, Z.H. Lu, Complete dehydrogenation of hydrazine borane and hydrazine catalyzed by MIL-101

supported NiFePd nanoparticles, J. Alloys Compd., 732 (2018) 363-371. http://doi.org/10.1016/j.jallcom.2017.10.241.

[27] Z.J. Zhang, S.L. Zhang, Q.L. Yao, X.S. Chen, Z.H. Lu, Controlled synthesis of MOF-encapsulated NiPt nanoparticles toward efficient and complete hydrogen evolution from hydrazine borane and hydrazine, Inorg. Chem., 56 (2017) 11938-11945. http://doi.org/10.1021/acs.inorgchem.7b01910.

[28] Y.X. Cheng, X. Wu, H. Xu, Catalytic decomposition of hydrous hydrazine for hydrogen production, Sustainable Energy Fuels, 3 (2019) 343-365. http://doi.org/10.1039/c8se00538a.

[29] F.Z. Song, X.C. Yang, Q. Xu, Ultrafine bimetallic Pt-Ni nanoparticles achieved by metal-organic framework templated zirconia/porous carbon/reduced graphene oxide: Remarkable catalytic activity in dehydrogenation of hydrous hydrazine, Small Methods, (2019) 1900707. http://doi.org/10.1002/smtd.201900707.

[30] Z.Q. Niu, Y.D. Li, Removal and utilization of capping agents in nanocatalysis, Chem. Mater., 26 (2014) 72-83. http://doi.org/10.1021/cm4022479.

[31] J.M. Yan, S.J. Li, S.S. Yi, B.R. Wulan, W.T. Zheng, Q. Jiang, Anchoring and upgrading ultrafine NiPd on room-temperature-synthesized bifunctional NH_2-N-rGO toward low-cost and highly efficient catalysts for selective formic acid dehydrogenation, Adv. Mater., 30 (2018) 1703038. http://doi.org/10.1002/adma.201703038.

[32] C. Wan, L. Sun, L.X. Xu, D.G. Cheng, F.Q. Chen, X.L. Zhan, Y.R. Yang, Novel NiPt alloy nanoparticle decorated 2D layered g-C_3N_4 nanosheets: a highly efficient

catalyst for hydrogen generation from hydrous hydrazine, J. Mater. Chem. A, 7 (2019) 8798-8804. http://doi.org/10.1039/c9ta01535c.

[33] X.J. Gu, Z.H. Lu, Q. Xu, High-connected mesoporous metal-organic framework, Chem. Commun., 46 (2010) 7400-7402. http://doi.org/10.1039/c0cc02808h.

[34] Q.L. Zhu, Q. Xu, Metal-organic framework composites, Chem. Soc. Rev., 43 (2014) 5468-5512. http://doi.org/10.1039/c3cs60472a.

[35] Z.B. Liang, R. Zhao, T.J. Qiu, R.Q. Zou, Q. Xu, Metal-organic framework-derived materials for electrochemical energy applications, EnergyChem, 1 (2019) 100001. http://doi.org/10.1016/j.enchem.2019.100001.

[36] Y.W. Yang, Z.H. Lu, Y.J. Hu, Z.J. Zhang, W.M. Shi, X.S. Chen, T.T. Wang, Facile in situ synthesis of copper nanoparticles supported on reduced graphene oxide for hydrolytic dehydrogenation of ammonia borane, RSC Adv., 4 (2014) 13749-13752. http://doi.org/10.1039/c3ra47023g.

[37] Q.L. Yao, Z.H. Lu, Y.W. Yang, Y.Z. Chen, X.S. Chen, H.L. Jiang, Facile synthesis of graphene-supported Ni-CeO_x nano-composites as highly efficient catalysts for hydrolytic dehydrogenation of ammonia borane, Nano Res., 11 (2018) 4412-4422. http://doi.org/10.1007/s12274-018-2031-y.

[38] J.M. Chen, Z.H. Lu, W. Huang, Z.B. Kang, X.S. Chen, Galvanic replacement synthesis of NiPt/graphene as highly efficient catalysts for hydrogen release from hydrazine and hydrazine borane, J. Alloys Compd., 695 (2017) 3036-3043. http://doi.org/10.1016/j.jallcom.2016.11.351.

[39] S.P. Wang, S.H. Hou, C. Wu, Y.J. Zhao, X.B. Ma, $RuCl_3$ anchored onto

post-synthetic modification MIL-101(Cr)-NH_2 as heterogeneous catalyst for hydrogenation of CO_2 to formic acid, Chin. Chem. Lett., 30 (2019) 398-402. http://doi.org/10.1016/j.cclet.2018.06.021.

[40] C. Petit, T.J. Bandosz, MOF-graphite oxide composites: Combining the uniqueness of graphene layers and metal-organic frameworks, Adv. Mater., 21 (2009) 4753-+. http://doi.org/10.1002/adma.200901581.

[41] D.D. Li, H.Q. Xu, L. Jiao, H.L. Jiang, Metal-organic frameworks for catalysis: State of the art, challenges, and opportunities, EnergyChem, 1 (2019) 100005. http://doi.org/10.1016/j.enchem.2019.100005.

[42] J.H. Fu, X.Y. Wang, T.T. Wang, J. Zhang, S. Guo, S. Wu, F.H. Zhu, Covalent functionalization of graphene oxide with a presynthesized metal-organic framework enables a highly stable electrochemical sensing, ACS Appl. Mater. Inter., 11 (2019) 33238-33244. http://doi.org/10.1021/acsami.9b10531.

[43] M. Muschi, C. Serre, Progress and challenges of graphene oxide/metal-organic composites, Coord. Chem. Rev., 387 (2019) 262-272. http://doi.org/10.1016/j.ccr.2019.02.017.

[44] Z.J. Zhang, Y.Q. Wang, X.S. Chen, Z.H. Lu, Facile synthesis of NiPt-CeO_2 nanocomposite as an efficient catalyst for hydrogen generation from hydrazine borane, J. Power Sources, 291 (2015) 14-19. http://doi.org/10.1016/j.jpowsour.2015.05.012.

[45] X.J. Sun, Q.B. Xia, Z.X. Zhao, Y.W. Li, Z. Li, Synthesis and adsorption performance of MIL-101(Cr)/graphite oxide composites with high capacities of n-hexane, Chem.

Eng. J., 239 (2014) 226-232. http://doi.org/10.1016/j.cej.2013.11.024.

[46] Z.H. Lu, J.P. Li, A.L. Zhu, Q.L. Yao, W. Huang, R.Y. Zhou, R.F. Zhou, X.S. Chen, Catalytic hydrolysis of ammonia borane via magnetically recyclable copper iron nanoparticles for chemical hydrogen storage, Int. J. Hydrogen Energy, 38 (2013) 5330-5337. http://doi.org/10.1016/j.ijhydene.2013.02.076.

[47] D.Y. Hong, Y.K. Hwang, C. Serre, G. Ferey, J.S. Chang, Porous chromium terephthalate MIL-101 with coordinatively unsaturated sites: surface functionalization, encapsulation, sorption and catalysis, Adv. Funct. Mater., 19 (2009) 1537-1552. http://doi.org/10.1002/adfm.200801130.

[48] S.J. Li, X. Kang, B.R. Wulan, X.L. Qu, K. Zheng, X.D. Han, J.M. Yan, Noble-metal-free Ni-MoO_x nanoparticles supported on BN as a highly efficient catalyst toward complete decomposition of hydrazine borane, Small Methods, 2 (2018). http://doi.org/10.1002/smtd.201800250.

[49] J.M. Chen, H.T. Zou, Q.L. Yao, M.H. Luo, X.G. Li, Z.H. Lu, Cr_2O_3-modified NiFe nanoparticles as a noble-metal-free catalyst for complete dehydrogenation of hydrazine in aqueous solution, Appl. Surf. Sci., 501 (2020) 144247. http://doi.org/10.1016/j.apsusc.2019.144247.

[50] Q. Shi, Y.P. Qiu, H. Dai, P. Wang, Study of formation mechanism of Ni-Pt/CeO_2 catalyst for hydrogen generation from hydrous hydrazine, J. Alloys Compd., 787 (2019) 1187-1194. http://doi.org/10.1016/j.jallcom.2019.01.378.

[51] K. Wang, Q.L. Yao, S.J. Qing, Z.H. Lu, $La(OH)_3$ nanosheet-supported CoPt nanoparticles: a highly efficient and magnetically recyclable catalyst for hydrogen

production from hydrazine in aqueous solution, J. Mater. Chem. A, 7 (2019) 9903-9911. http://doi.org/10.1039/c9ta01066a.

[52] H.L. Wang, J.M. Yan, Z.L. Wang, S.I. O, Q. Jiang, Highly efficient hydrogen generation from hydrous hydrazine over amorphous $Ni_{0.9}Pt_{0.1}/Ce_2O_3$ nanocatalyst at room temperature, J. Mater. Chem. A, 1 (2013) 14957-14962. http://doi.org/10.1039/c3ta13259e.

[53] J.J. Zhang, Q. Kang, Z.Q. Yang, H.B. Dai, D.W. Zhuang, P. Wang, A cost-effective NiMoB-$La(OH)_3$ catalyst for hydrogen generation from decomposition of alkaline hydrous hydrazine solution, J. Mater. Chem. A, 1 (2013) 11623-11628. http://doi.org/10.1039/c3ta12528a.

[54] B.Q. Xia, N. Cao, H.M. Dai, J. Su, X.J. Wu, W. Luo, G.Z. Cheng, Bimetallic nickel-rhodium nanoparticles supported on ZIF-8 as highly efficient catalysts for hydrogen generation from hydrazine in alkaline solution, ChemCatChem, 6 (2014) 2549-2552. http://doi.org/10.1002/cctc.201402353.

[55] B.Q. Xia, T. Liu, W. Luo, G.Z. Cheng, NiPt-MnO_x supported on N-doped porous carbon derived from metal-organic frameworks for highly efficient hydrogen generation from hydrazine, J. Mater. Chem. A, 4 (2016) 5616-5622. http://doi.org/10.1039/c6ta00766j.

[56] T.W. van Deelen, C.H. Mejia, K.P. de Jong, Control of metal-support interactions in heterogeneous catalysts to enhance activity and selectivity, Nat. Catal., 2 (2019) 955-970. http://doi.org/10.1038/s41929-019-0364-x.

[57] H.T. Zou, F. Guo, M.H. Luo, Q.L. Yao, Z.H. Lu, $La(OH)_3$-decorated NiFe

nanoparticles as efficient catalyst for hydrogen evolution from hydrous hydrazine and hydrazine borane, Int. J. Hydrogen Energy, 45 (2020) 11641-11650. https://doi.org/10.1016/j.ijhydene.2020.02.074.

[58] J.M. Chen, Z.H. Lu, Q.L. Yao, G. Feng, Y. Luo, Complete dehydrogenation of $N_2H_4BH_3$ with NiM-Cr_2O_3 (M = Pt, Rh, and Ir) hybrid nanoparticles, J. Mater. Chem. A, 6 (2018) 20746-20752. http://doi.org/10.1039/c8ta08050j.

[59] S.J. Li, H.L. Wang, B.R. Wulan, X.B. Zhang, J.M. Yan, Q. Jiang, Complete dehydrogenation of $N_2H_4BH_3$ over noble-metal-free $Ni_{0.5}Fe_{0.5}$-CeO_x/MIL-101 with high activity and 100% H_2 selectivity, Adv. Energy. Mater., 8 (2018). http://doi.org/10.1002/aenm.201800625.

[60] S.L. Zhang, Q.L. Yao, Q.Y. Li, G. Feng, Z.H. Lu, Complete hydrogen production from hydrazine borane over raney Ni catalyst at room temperature, Energy Technol, 7 (2019) 1800533. http://doi.org/10.1002/ente.201800533.

[61] K.K. Yang, Q.L. Yao, W. Huang, X.S. Chen, Z.H. Lu, Enhanced catalytic activity of NiM (M = Cr, Mo, W) nanoparticles for hydrogen evolution from ammonia borane and hydrazine borane, Int. J. Hydrogen Energy, 42 (2017) 6840-6850. http://doi.org/10.1016/j.ijhydene.2016.12.029.

List of figure captions

Scheme 1 Schematic illustration for the preparation of NiPt/MIL-101/rGO catalyst.

Fig. 1 (a) Low-angle and (b) wide-angle XRD patterns of MIL-101/GO, Ni/MIL-101/rGO, NiPt/MIL-101/rGO, and Pt/MIL-101/rGO.

Fig. 2 XPS spectra of (a) Ni 2p and (b) Pt 4f for $Ni_{0.9}Pt_{0.1}$/MIL-101/rGO catalyst after argon sputtering for 5 min.

Fig. 3 (a,b) SEM images of the as-prepared GO and MIL-101 samples. (c,d) Low resolution TEM images, (e) high resolution TEM image, and (f) SAED pattern of the $Ni_{0.9}Pt_{0.1}$/MIL-101/rGO catalyst.

Fig. 4 Nitrogen adsorption-desorption isotherms of the as-prepared MIL-101, MIL-101/GO, and $Ni_{0.9}Pt_{0.1}$/MIL-101/rGO samples after dehydration under vacuum at 373 K for 8 h.

Fig. 5 (a) Time-course plots and (b) the corresponding TOF values for hydrogen evolution from $N_2H_4 \cdot H_2O$ catalyzed by MIL-101/GO, $Ni_{0.9}Pt_{0.1}$, $Ni_{0.9}Pt_{0.1}$/rGO, $Ni_{0.9}Pt_{0.1}$/MIL-101, and $Ni_{0.9}Pt_{0.1}$/MIL-101/rGO in the presence of NaOH (1.0 M) at 323 K ($n_{Ni+Pt}/n_{N_2H_4 \cdot H_2O} = 0.05$).

Fig. 6 (a) Time-course plots and (b) the corresponding TOF values and H_2 selectivity for hydrogen evolution from $N_2H_4 \cdot H_2O$ catalyzed by Ni_xPt_{1-x}/MIL-101/rGO ($0 \leq x \leq 1.0$) in the presence of NaOH (1.0 M) at 323 K ($n_{Ni+Pt}/n_{N_2H_4 \cdot H_2O} = 0.05$).

Fig. 7 Time-course plots and its related Arrhenius plots for hydrogen evolution from (a,b) $N_2H_4 \cdot H_2O$ and (c,d) $N_2H_4BH_3$ catalyzed by $Ni_{0.9}Pt_{0.1}$/MIL-101/rGO at different temperatures.

Fig. 8 Durability tests of $Ni_{0.9}Pt_{0.1}$/MIL-101/rGO catalyst for hydrogen evolution from (a) $N_2H_4 \cdot H_2O$ and (b) $N_2H_4BH_3$ at 343 K.

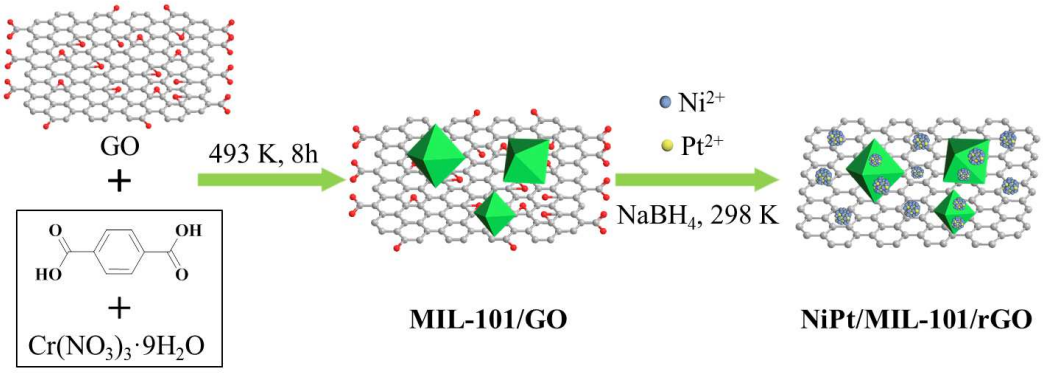

Scheme 1 Schematic illustration for the preparation of NiPt/MIL-101/rGO catalyst.

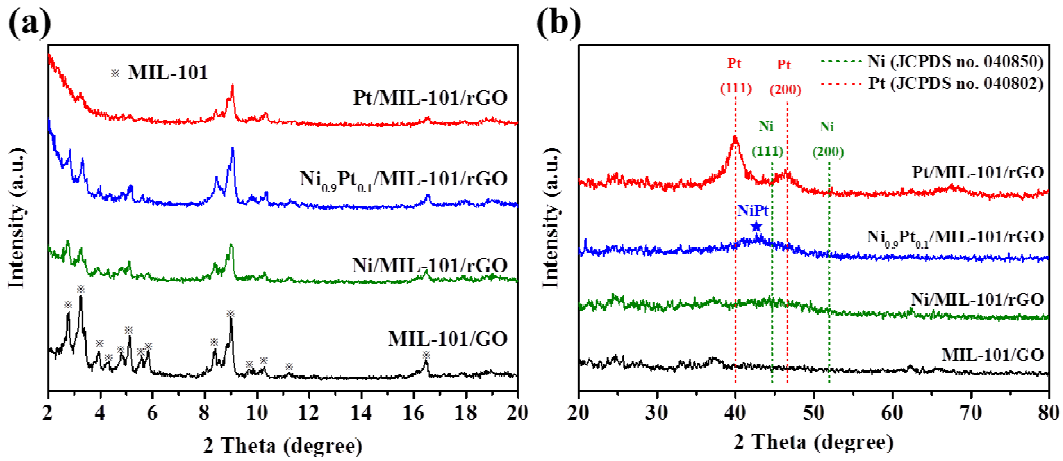

Fig. 1 (a) Low-angle and (b) wide-angle XRD patterns of MIL-101/GO, Ni/MIL-101/rGO, NiPt/MIL-101/rGO, and Pt/MIL-101/rGO.

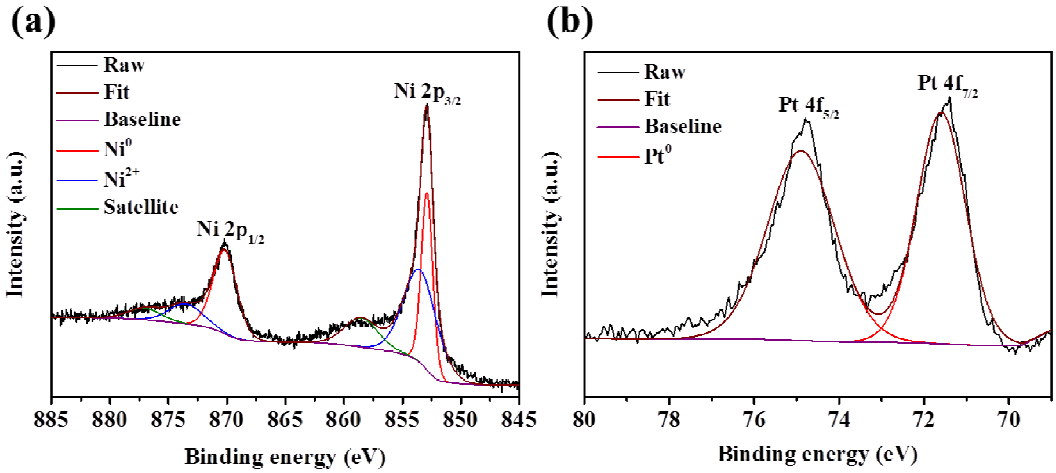

Fig. 2 XPS spectra of (a) Ni 2p and (b) Pt 4f for $Ni_{0.9}Pt_{0.1}$/MIL-101/rGO catalyst after argon sputtering for 5 min.

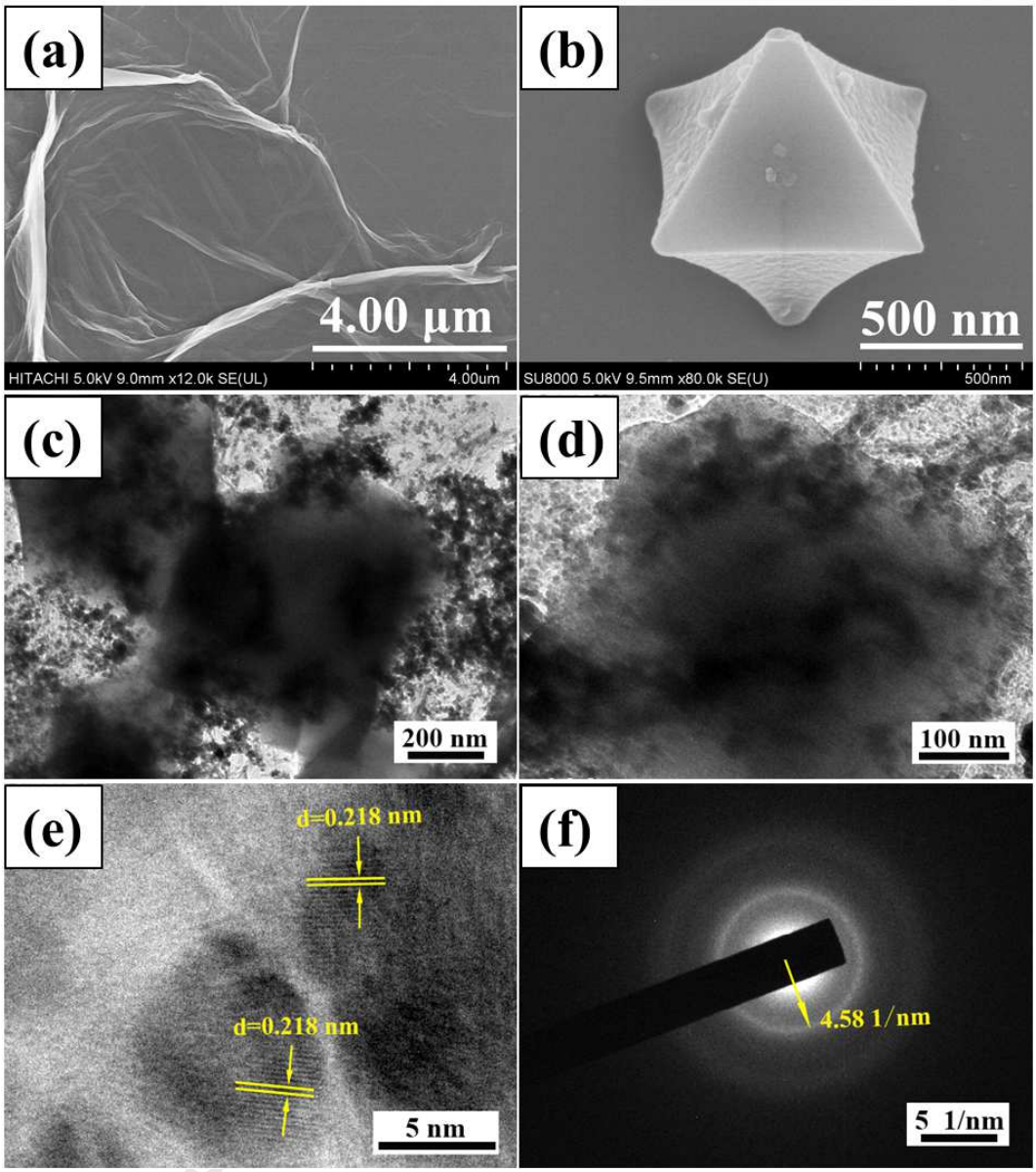

Fig. 3 (a,b) SEM images of the as-prepared GO and MIL-101 samples. (c,d) Low resolution TEM images, (e) high resolution TEM image, and (f) SAED pattern of the $Ni_{0.9}Pt_{0.1}$/MIL-101/rGO catalyst.

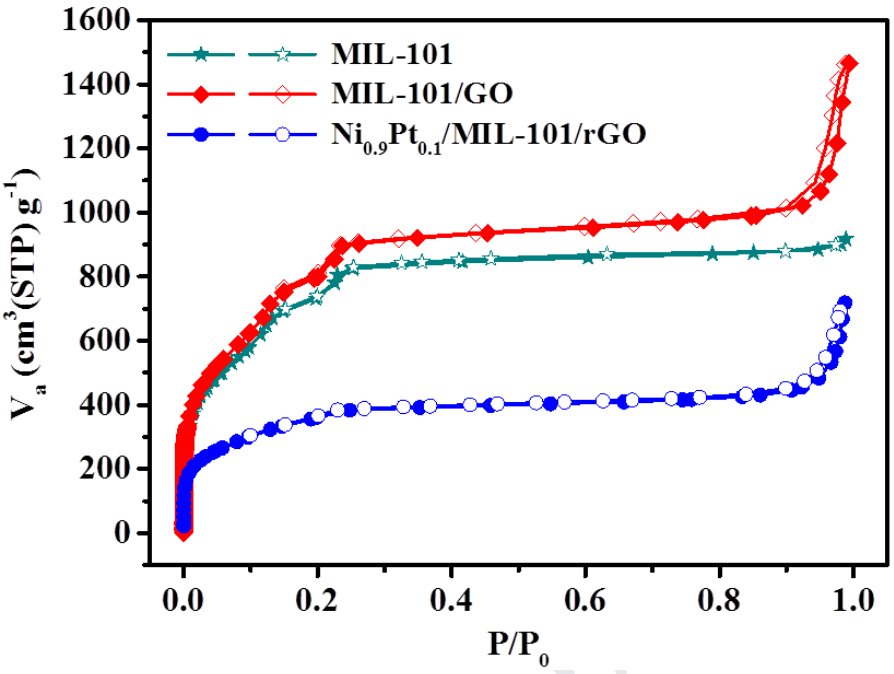

Fig. 4 Nitrogen adsorption-desorption isotherms of the as-prepared MIL-101, MIL-101/GO, and $Ni_{0.9}Pt_{0.1}$/MIL-101/rGO samples after dehydration under vacuum at 373 K for 8 h.

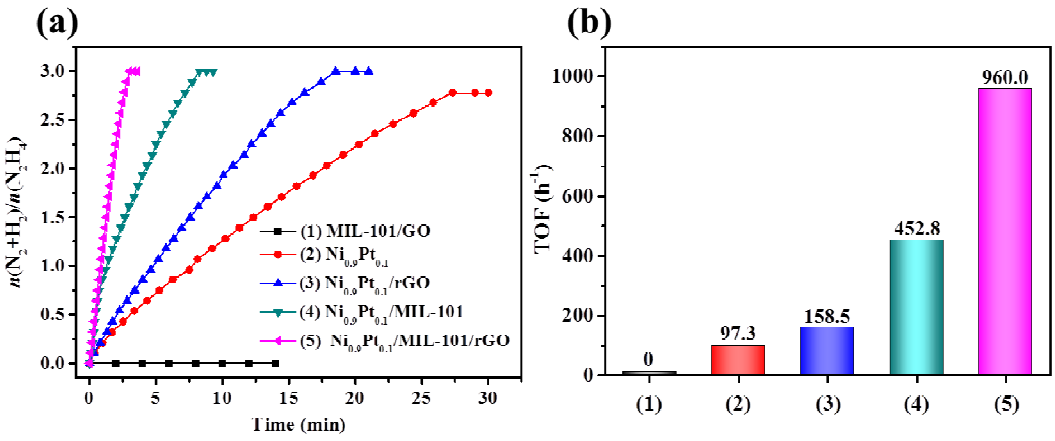

Fig. 5 (a) Time-course plots and (b) the corresponding TOF values for hydrogen evolution from $N_2H_4 \cdot H_2O$ catalyzed by MIL-101/GO, $Ni_{0.9}Pt_{0.1}$, $Ni_{0.9}Pt_{0.1}$/rGO, $Ni_{0.9}Pt_{0.1}$/MIL-101, and $Ni_{0.9}Pt_{0.1}$/MIL-101/rGO in the presence of NaOH (1.0 M) at 323 K ($n_{Ni+Pt}/n_{N_2H_4 \cdot H_2O} = 0.05$).

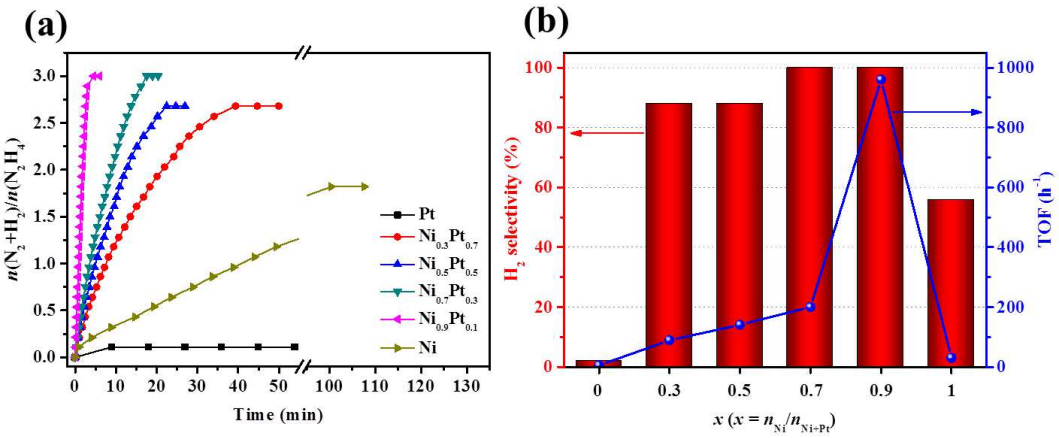

Fig. 6 (a) Time-course plots and (b) the corresponding TOF values and H_2 selectivity for hydrogen evolution from $N_2H_4 \cdot H_2O$ catalyzed by Ni_xPt_{1-x}/MIL-101/rGO ($0 \leq x \leq 1.0$) in the presence of NaOH (1.0 M) at 323 K ($n_{Ni+Pt}/n_{N_2H_4 \cdot H_2O} = 0.05$).

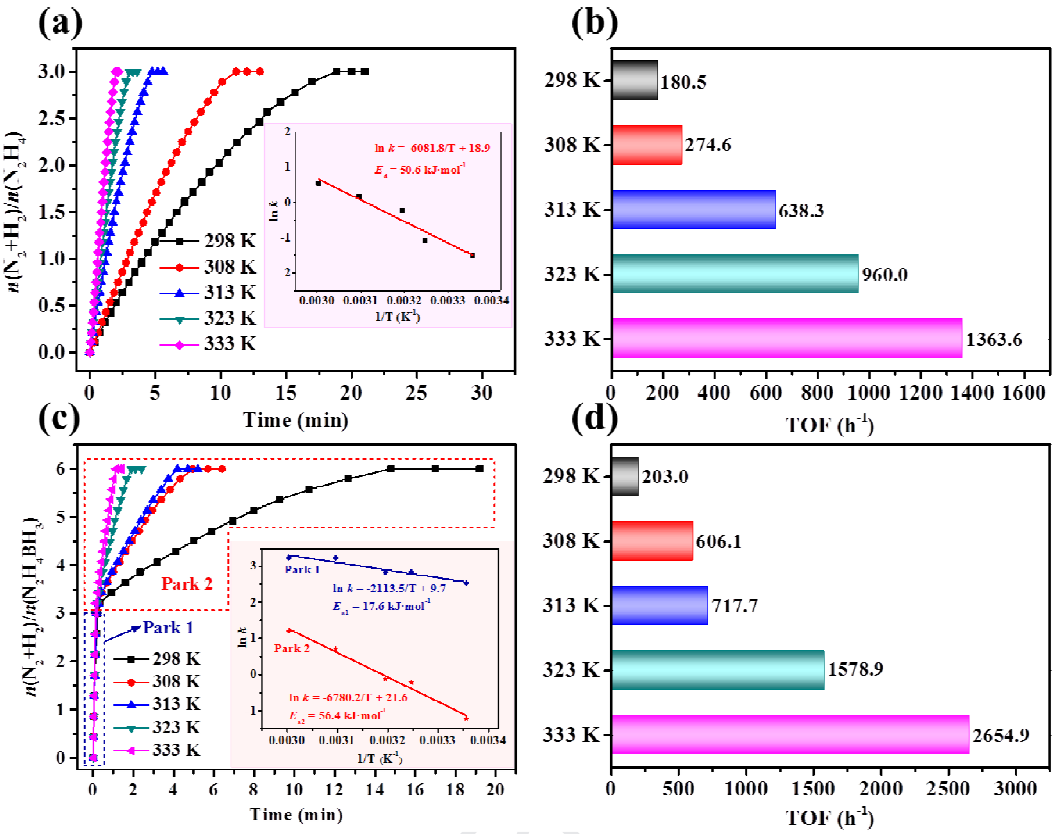

Fig. 7 Time-course plots and its related Arrhenius plots for hydrogen evolution from (a,b) $N_2H_4 \cdot H_2O$ and (c,d) $N_2H_4BH_3$ catalyzed by $Ni_{0.9}Pt_{0.1}$/MIL-101/rGO at different temperatures.

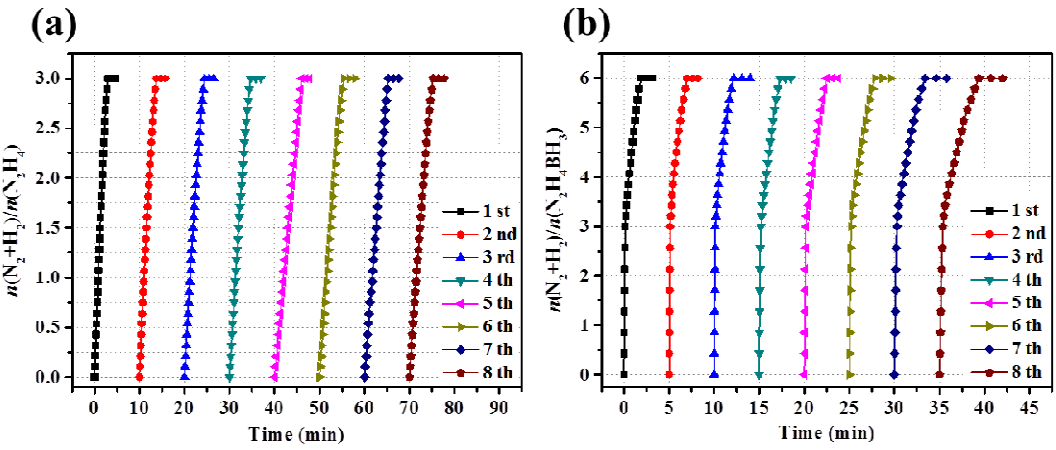

Fig. 8 Durability tests of $Ni_{0.9}Pt_{0.1}$/MIL-101/rGO catalyst for hydrogen evolution from (a) $N_2H_4 \cdot H_2O$ and (b) $N_2H_4BH_3$ at 343 K.

Highlights

- $Ni_{0.9}Pt_{0.1}$/MIL-101/rGO catalyst was prepared via a wet-chemical method.
- This catalyst has a unique structure and large specific surface area.
- $Ni_{0.9}Pt_{0.1}$/MIL-101/rGO exhibits high activity, selectivity and durability.
- TOF value of 960.0 for N_2H_4 dehydrogenation was achieved at 323 K.
- Activation energy for N_2H_4 dehydrogenation is estimated to 50.6 $kJ \cdot mol^{-1}$.

Declaration of interests

☐✓ The authors declare that they have no known competing financial interests or personal relationships that could have appeared to influence the work reported in this paper.

☐The authors declare the following financial interests/personal relationships which may be considered as potential competing interests: